

# Studies on the Mechanical, Electrical Properties and Interaction of Petroleum Fuels with SBR/ Manganous Tungstate Nanocomposites

V. C. Jasna<sup>1</sup> · M. T. Ramesan<sup>1</sup>

Received: 13 March 2017 / Accepted: 5 April 2017 / Published online: 9 April 2017  
© Springer Science+Business Media New York 2017

**Abstract** A novel nanocomposite based on styrene butadiene rubber (SBR) and manganous tungstate ( $\text{MnWO}_4$ ) nanoparticles was prepared by a simple and inexpensive open two-roll mixing mill. The interaction of the nanoparticles with SBR matrix was studied by different characterization techniques such as X-ray diffraction (XRD), scanning electron microscopy (SEM), thermogravimetric analysis (TGA) and electrical properties. The effect of loading of  $\text{MnWO}_4$  nanoparticles on the processing characteristics of mixed rubber compounds, mechanical properties and the transport properties of nanocomposites through petroleum fuels were also analysed. XRD of nanocomposite revealed that the addition of nanoparticles imparts a semi-crystalline or regular arrangement of chains in the composite. SEM analysis showed good dispersion of nanoparticles in the polymer matrix. Also it has been observed that the dispersion of nanoparticles decreases with increase in its loading. TGA analysis indicated better thermal stability of all nanocomposite and thermal stability increases with the loading of the nanoparticles. The AC conductivity and dielectric properties were greatly enhanced in the whole range of frequencies studied. The processing properties of rubber compounds like cure and scorch time decreases with increase in concentration of  $\text{MnWO}_4$  nanoparticles and the maximum enhancement in torque was observed for 10 phr loading. The tensile strength, modulus, tear resistance, hardness and heat build-up of the composite increased whereas the resilience, compression set and elongation at break decreased with the loading of nanoparticles. Solvent penetration

studies of nanocomposites were done in petroleum fuels at different temperatures. The solvent uptake was the minimum for composite with 10 phr of  $\text{MnWO}_4$  and penetration of solvent increased with further addition of nanoparticles.

**Keywords** SBR · Manganous tungstate nanoparticles · Crystallinity · Thermal stability · Electrical studies · Mechanical properties · Petroleum fuels

## 1 Introduction

One of the most accepted and widely used strategies for improving the mechanical and thermal properties of soft elastomers is through the incorporation of inorganic materials especially in the form of nanoparticles. While a minimum of 30–60 weight percentage of conventional micro sized fillers are needed to improve the mechanical properties of elastomers, only a few percentages (3–15 wt%) of nanoparticles can serve the same purpose more effectively [1, 2]. It is already known that a higher loading of filler particles causes a hike in the weight and density of the final product while it also reduces the processability of the elastomer composite. In addition, as well as in many developing and developed countries, there has been a continuous demand for novel light weight with high performing elastomer composites. They must satisfy increasingly stringent requirements such as high tensile strength, modulus, thermal stability and exceptional electrical properties [3]. Polymer nanocomposites are unchallenging candidates till today for many special applications and are much superior to conventionally filled elastomer composites. Nano-phase dimension can do wonders in such roles due to their unique properties which are not shared by their conventional micro-composites and therefore it offers new technology

✉ M. T. Ramesan  
mtramesan@uoc.ac.in

<sup>1</sup> Department of Chemistry, University of Calicut, Calicut University P.O, Malappuram, Kerala 673 635, India

and business opportunities. The addition of nanoparticles increases the physical properties of polymers with even small amounts of filler particles [4, 5]. A large number of nano-fillers are currently used in rubber industry to improve the mechanical properties of elastomeric products. Researches on semiconducting nanoparticles are of much interest in recent years because of their unique optical and electrical properties [6, 7].

Apart from their use in unique and special applications, polymers are widely used in packaging. But it may sometimes chemically react or dissolve and may diffuse into the system. Rubber in its original form will dissolve in aromatic and industrial solvents. In order to prepare best performing elastomer products, it is very important to reinforcing them with appropriate compounding of particulate fillers [8]. Addition of fillers especially nano-fillers to the elastomer matrix, the transport of solvent molecules through the polymer membrane can be decreased. The diffusion and transport study of different organic and industrial solvents through polymer composite containing clay as filler generated many interesting research works and resulted in useful for the mankind [9]. Filler addition to the polymer matrix can cause a decrease in diffusion and permeation of solvent molecules through polymer matrix. The rate of diffusion depends on the various factors such as amount of filler, temperature, penetrant size, interfacial interaction between filler and matrix etc. [10–13]. The addition of filler to the polymer matrix will reduce the free volume inside the matrix and this will cause a decrease in diffusion rate. The decrease in swelling is mainly due to the intense interaction between the filler and polymer matrix. Several works were carried out to verify the importance of filler in diffusion study. It is generally found that the incorporation of filler with polymer matrix reduces the diffusion and permeation process of hydrocarbons into polymer matrices [14–16].

Styrene butadiene rubber (SBR) is a widely used synthetic rubber, with numerous industrial applications resulting mainly from its excellent abrasion resistance. The main area of its application is in tyre industry, shoes soles and in gasket production. In the case of tyre production, attention must be done otherwise high amount of heat will produce at the time of running on the road, it will produce high friction and may cause degradation of tyre. Proper compounding, mixing and curing are very important to get best quality products [17, 18]. Many types of fillers like calcium carbonate, clay, silica, carbon black etc. are generally used for the reinforcement of elastomers. The interaction between rubber and filler particles will impart strength and improved properties to the composites. The interfacial interaction between polymer matrix and filler may be due to some van der Waals type of force between them. Generally van der Waals forces cause adhesive forces between elastomer and fillers. In order to prepare stronger and high

performing elastomer composites, the above interfacial interaction must be much stronger. This can be achieved only through the chemical interaction between functional group on the surface of fillers and in the elastomers [19]. This work focused on the incorporation of  $\text{MnWO}_4$  nanoparticles into SBR to study the interaction of  $\text{MnWO}_4$  nanoparticles with SBR matrix and its role in altering the mechanical, electrical and transport properties of petroleum hydrocarbons. To the best of our knowledge, there is no report in the literature regarding the preparation of SBR/ $\text{MnWO}_4$  nanocomposite. In this study a simple and inexpensive two roll mill mixing technique is used for the fabrication of SBR based nanocomposites. The structure and morphology of the composites were studied using XRD and SEM. The effect of metal nanoparticles on processing characteristics, thermal, mechanical and electrical properties of the nanocomposite has been investigated. Petroleum hydrocarbons such as petrol, diesel, and kerosene are possible threats to SBR in automobile applications, so the present study also evaluates the transport properties of SBR/ $\text{MnWO}_4$  nanocomposite vulcanizates.

## 2 Experimental

### 2.1 Materials and Methods

SBR (Synaprene 1502) was obtained from Synthetics and Chemicals Ltd., Bareilly, UP., India. Manganous chloride, sodium tungstate and cetyl trimethyl ammonium bromide (CTAB) were purchased from Himedia chemicals. The technical grade ingredients like zinc oxide (ZnO), stearic acid, 2,2,4-trimethyl-1,2-dihydroquinoline (TDQ), cyclohexyl benzothiazole (CBS), processing oil and sulphur have been used for this study without further purifications.

### 2.2 Synthesis of $\text{MnWO}_4$ Nanopowder

$\text{MnWO}_4$  nanoparticles were prepared by the chemical coprecipitation technique as described earlier [20]. Equimolar quantities of manganous chloride and sodium tungstate were dissolved in distilled water individually. Then cetyl trimethyl ammonium bromide was added to the manganous chloride solution with continuous stirring. The sodium tungstate solution was added drop wise to the chloride/CTAB mixture and kept in stirring. The precipitate formed was washed with water several times and dried at 100 °C for 2 h. The dried powder was calcined at 800 °C for 5 h.

### 2.3 Preparation of SBR/ $\text{MnWO}_4$ Nanocomposites

$\text{MnWO}_4$  nanoparticles with different weight ratios of 0, 3, 5, 7, 10 and 15 phr (parts per hundred parts rubber)

was mixed with SBR (100 gm) in an open two roll mixing mill. Composite materials were prepared by adding 5.0 phr ZnO, 2.0 phr stearic acid, 1.0 phr TDQ, processing oil 1/20th of filler, 1.2 phr CBS and 2.4 phr sulphur to rubber. Compounding was carried out at 28 °C in accordance with relevant ASTM standards with a special attention to maintain the uniform distribution of nanoparticles. Here we use the sample code as SM<sub>0</sub> is SBR with no filler loading SM<sub>3</sub>, SM<sub>5</sub>, SM<sub>7</sub>, SM<sub>10</sub> and SM<sub>15</sub> are rubber composite with 3, 5, 7, 10 and 15 phr of MnWO<sub>4</sub> nanoparticles.

## 2.4 Characterizations

X-ray diffraction analysis was done using RIGAKU MINI-FLEX-600 diffractometer. The diffractogram was recorded in terms of  $2\theta$  in the range 10°–80°. Thermal decomposition behaviour of the nanocomposite was studied using Perkin Elmer thermo gravimetric analyzer at a heating rate of 10 °C/min. in an inert atmosphere. The surface morphology of the nanocomposite was analysed by field emission scanning electron microscope (Hitachi, SU 6600FESEM). The alternating current (AC) and dielectric loss of the elastomeric materials were measured by automatic Hewlett Packard LCR meter (HP: 4284 A) in the frequency range 10<sup>2</sup>–10<sup>6</sup> Hz. Cure characteristics were studied by a Monsanto Rheometer R-100 at 150 °C according to ASTM D 2705. The samples were moulded in an electrically heated hydraulic press at a pressure of 40 MPa for the respective optimum cure times. Dumb-bell specimens were punched out from the moulded sheets. The tensile strength and tear resistance of the samples were carried out using a Zwick Universal Testing Machine (UTM) at 28 °C and at a cross-head speed of 500 mm/min according to ASTM D 412-80 and ASTM D 624-81 respectively. Hardness of the compound was measured according to ASTM D 2240-95 using a Shore A type durometer. The rebound resilience was determined using a Dunlop Tripsometer, as per ASTM D 1054. The compression set values were determined by the constant strain method keeping the compound for 22 h at 70 °C, according to ASTM D 395-89 method B. Heat build-up of the sample was determined by Goodrich flexometer according to ASTM D 623. The abrasion resistance of the samples was tested using a DIN abrader according to DIN 5351 procedure. The diffusion and transport mechanism of SBR/MnWO<sub>4</sub> nanocomposites was also done gravimetrically using circular samples which were punched out from the vulcanized samples using sharp edged steel die. The thickness of the sample was measured using a screw gauge and the weighed samples were immersed in different hydrocarbon solvents like petrol, diesel and kerosene taken in the diffusion bottles. Weigh the samples in particular time intervals and again put in the solvents. The weighing of sample was continued until the equilibrium weight

was obtained. And the solvent uptake experiments were repeated at different temperatures.

## 3 Results and Discussion

### 3.1 X-ray Diffraction Analysis (XRD)

The XRD profile of MnWO<sub>4</sub>, SBR and SBR with 5 and 15 phr of MnWO<sub>4</sub> filled SBR nanocomposites are presented in Fig. 1. The crystalline peaks of MnWO<sub>4</sub> are visible at several regions in the XRD curve indicating the highly crystalline nature of the nanoparticles [21]. The broad peak at  $2\theta=20.7^\circ$  indicates the amorphous nature of SBR. The XRD pattern of nanocomposites shows most of the crystalline peaks of MnWO<sub>4</sub> along with amorphous peak of SBR. It is important to mention here that the broadness of the amorphous peak of SBR decreases with increase in concentration of nanoparticles. Also the position of amorphous peak slightly shifts to lower  $2\theta$  region (i.e., from  $2\theta=20.7^\circ$  to  $17.88^\circ$  for 5phr composite). The decrease in amorphous nature of nanocomposite with the loading of fillers is due to the strong interfacial interaction between the nanoparticles and polymer chain. Hence it can be understood from the results that the introduction of MnWO<sub>4</sub> nanoparticles in to SBR reduces the amorphous structure of the polymer matrix.

### 3.2 Scanning Electron Microscopy (SEM)

The morphology of SBR and SBR with 7 and 15 phr of MnWO<sub>4</sub> filled nanocomposites are studied by SEM and are exhibited in Fig. 2. It can be observed that the compact morphology of SBR has slightly changed in to more relaxed phase morphology by the addition of MnWO<sub>4</sub> nanoparticles. Several nanoparticles are uniformly dispersed in SBR (Fig. 2b) and this indicates the good interaction of nanoparticles with the macromolecular chain of SBR. However at higher loading of nanoparticles (Fig. 2c), the uniform dispersion of nanoparticles has totally changed into aggregate structures. On this basis, it can be suggested that the aggregation of nanoparticles at higher loading restrict the polymer filler interaction and this leads to the sedimentation of filler particles.

### 3.3 Thermogravimetric Analysis (TGA)

TGA curve of the thermal degradation behaviour of SBR with 5, 10 and 15 phr of MnWO<sub>4</sub> nanoparticles are shown in Fig. 3. The results show the thermal stability of nanocomposite is clearly enhanced by the incorporation of nanoparticles and all the samples show a single stage decomposition pattern. The thermal degradation of SBR as usual

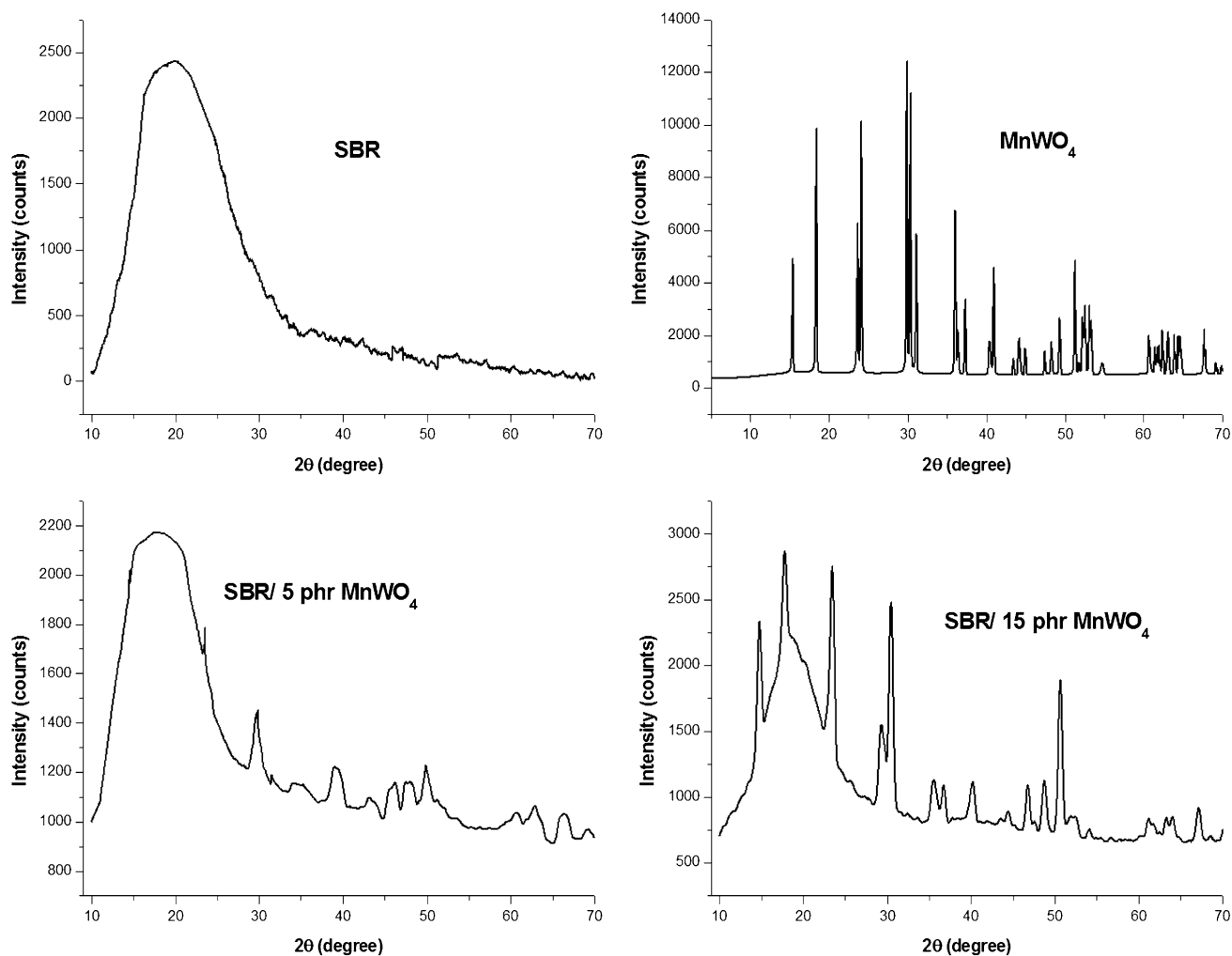


**Fig. 1** XRD pattern of  $\text{MnWO}_4$ , SBR and different content of  $\text{MnWO}_4$  containing SBR

is observed at  $401^\circ\text{C}$ . The composite with 5, 10 and 15 phr are undergoing thermal decomposition comparatively to higher temperature, i.e. at  $411$ ,  $422$  and  $429^\circ\text{C}$  respectively. The decomposition temperature of 10 phr of composite is raised by  $21^\circ\text{C}$  as compared to that of pure SBR. The increase in thermal stability with increase in loading of nanoparticle supports the higher interfacial interaction between nanoparticles and the polymer chain. Since the nanoparticles possess large effective surface area can effectively interact with SBR chains and this interaction can lead to a protective layer on the surface of polymer matrix. This restricts further thermal degradation of composite materials. Moreover the final char residue left after  $700^\circ\text{C}$  for pure SBR is only 9.21%, while for the composites with 5, 10 and 15 phr nanoparticle loading; the values are 14.11, 18.09 and 13.52% respectively. The high char residue obtained for 10 phr loading is due to the increased interfacial interaction between polymer and filler. The decrease in char residue of 15 phr composite as compared to 10 phr

loading is mainly arises from the poor adhesion that leads to aggregation of filler particles and this result is in good agreement with the SEM analysis. The increased value of char residue is an indication of the improved flame resistance of polymer composites [22].

### 3.4 AC conductivity

Figure 4 shows the AC electrical properties of SBR and SBR with different contents of  $\text{MnWO}_4$  nanoparticles at various frequencies. It is found that the AC conductivity of all the composites is much higher than pure SBR. The AC conductivity of all the samples increases with increase in frequency. The frequency dependence of AC conductivity is explained on the basis of Maxwell-Wagner two layer models and the highly crystalline structure of  $\text{MnWO}_4$  nanoparticles. It is well clear from the figure that the increasing trend of AC conductivity is steeper at higher frequencies and this is related to the conductive grains present in

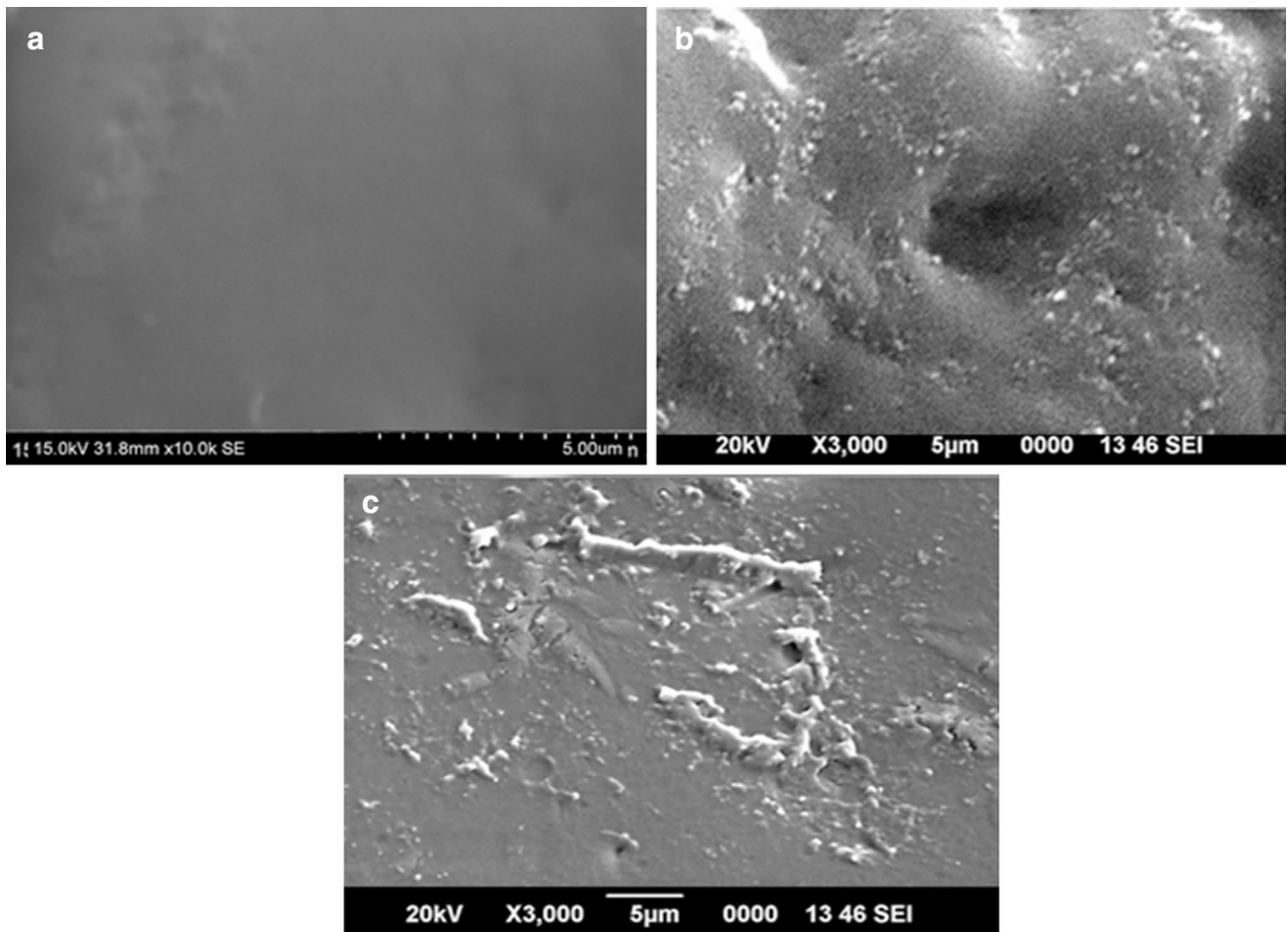


**Fig. 2** SEM images of **a** SBR **b** SBR with 7 phr and **c** SBR with 15 phr MnWO<sub>4</sub> nanoparticles

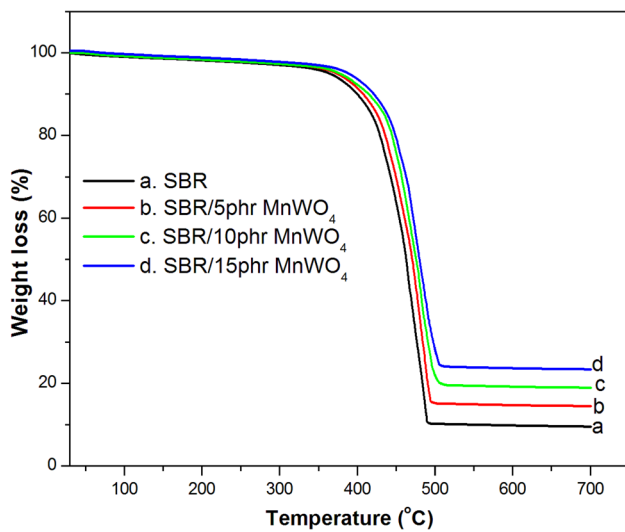


**Fig. 3** TGA curve of SBR and SBR with different content of MnWO<sub>4</sub> nanoparticles

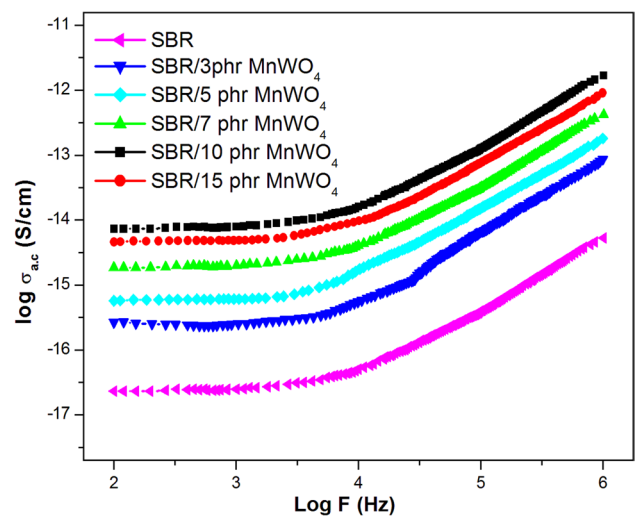


**Fig. 4** AC conductivity of SBR and SBR with different content of MnWO<sub>4</sub> nanoparticles

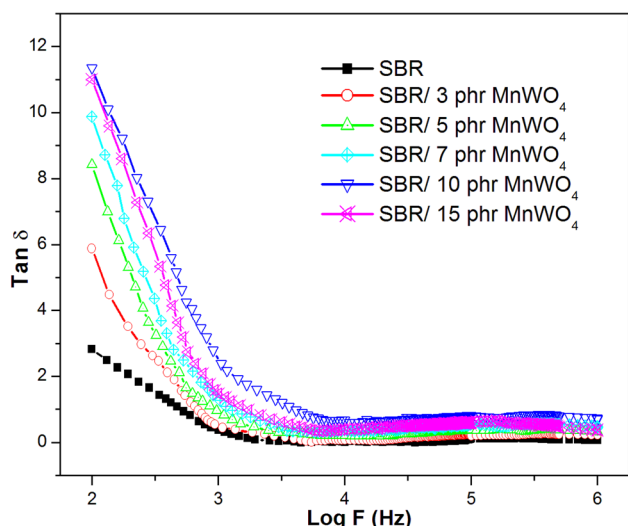


**Fig. 5** Dielectric loss tangent plots of SBR and SBR/MnWO<sub>4</sub> nanocomposite

**Table 1** Processing characteristics of SBR and SBR with different loading of MnWO<sub>4</sub> nanoparticles

Sample code	Cure time, t <sub>90</sub> (min)	Scorch time, t <sub>2</sub> (min)	Maximum torque (dNm)	Minimum torque (dNm)
SM <sub>0</sub>	15.7	4.8	29	6.9
SM <sub>3</sub>	15.0	4.5	31	7.3
SM <sub>5</sub>	14.3	4.13	34	7.7
SM <sub>7</sub>	13.8	3.84	36	7.9
SM <sub>10</sub>	13.2	3.52	39	8.3
SM <sub>15</sub>	12.8	3.22	38	8.2

the system. The overall AC conductivity of nanocomposite increases with increase in loading of nanoparticles. In the case of nanocomposite, the higher conductivity is either due to hopping of charge carriers between Mn<sup>3+</sup> and Mn<sup>2+</sup> ions. The hopping of charge carrier increases not only with frequencies but also with the loading of filler particles. Hence it can be inferred that the addition of MnWO<sub>4</sub> nanoparticles into the rubber matrix impart bulk conductivity to SBR, and the bulk conductivity depends on the concentration, filler-polymer interaction and the dispersion of nanoparticles [23]. The maximum conductivity is noted for 10 phr of MnWO<sub>4</sub> filled nanocomposite. This means that the nanoparticles are effectively interacting with the SBR chains. As the interfacial adhesion increases in the composites, the nanoparticles are more tightly packed and pressed against each other and this leads to the uniform orientation of nanoparticles within the polymer chain. The decrease in AC conductivity beyond 10 phr loading is due to the increase in the net resistance, resulting from the poor adhesion between filler and polymer. Moreover

the heterogeneous structure developed from the aggregate or clusters like morphology resist the hopping of electrons throughout the matrix and thereby causes a decrease in AC conductivity.

### 3.5 Dielectric Loss (Tan δ)

The dissipation factor of SBR/MnWO<sub>4</sub> nanocomposite was observed by plotting the tan δ versus frequency with different loading of nanoparticles and which is shown in Fig. 5. The dissipation factor of nanocomposite is higher than pure SBR and the tan δ value increases with the loading of nano-fillers. The increase in tan δ value is mainly attributed to the formation of interfacial polarisation by the addition of MnWO<sub>4</sub> particles. Tan δ value is found to decrease steeply with increase in frequency and reaches a constant value at 10<sup>4</sup> Hz for all samples in the present investigation. At lower frequencies, the inertia of molecules and the binding forces are low and therefore charge carriers easily flow with the application of electric field. Hence the dielectric loss shows a large tan δ value at lower frequency. However at higher frequencies, the charge carriers do not get enough time for long range hopping before field reversal. Therefore tan δ decreases as the signal frequency increases [24]. It can be seen from the figure that the dielectric loss increases with increase in concentration of filler particles upto 10 phr of loading. This indicates that the electron exchange between Mn<sup>3+</sup> and Mn<sup>2+</sup> ions in the composite affect the local displacement of electrons in the direction of applied field, results in an enhanced polarisation at this loading. This interaction is responsible for the higher tan δ value of 10 phr composite. The decrease in tan δ value above 10 phr loading is due to the presence of aggregate or cluster in the nanocomposites (which is well clear from the SEM images) and these aggregates reduce the hopping of charge carriers in the polymer matrix.

### 3.6 Processing Characteristics

Table 1 represents the effect of different content of MnWO<sub>4</sub> nanoparticles on the curing or processing characteristics of SBR. It is clear that the scorch time and optimum cure time decreases with increase in loading of nanoparticles in SBR. The decrease in cure properties as compared to pure SBR is due to the increased conducting nature of metal particles present in the composite. Also the polymer matrix becomes more viscous and heated with the addition of nanoparticles, which shortens the optimum cure time. The variation of torque (maximum and minimum torque) increases significantly with increase in loading of nanoparticles in SBR. The increase in rheometric torque is an indication of the crosslinking of the nanocomposite [25]. It is interesting to observe that the increase in torque is more pronounced at 10

phr filler loading and thereafter the torque value decreases with further addition of nanoparticles. It is well known that the maximum torque depends on the crosslink density which is directly related to the greater interaction between the filler and rubber matrix. The decrease in torque value at higher loading is attributed to the formation of individual cluster in the polymer composite.

### 3.7 Effect of Nanoparticles on Mechanical Properties

Tensile strength measurement has a major role among the other mechanical properties because the composite having higher tensile strength seem to be more durable and perform well in daily service. The effect of  $\text{MnWO}_4$  nanoparticles on the mechanical properties of SBR are summarised in Table 2. The tensile strength and modulus (at 300% elongation) of composite increased with the loading of nanoparticles up to 10 phr. Higher tensile strength and tensile modulus of nanocomposite is due to the homogeneous dispersion of nanoparticles in SBR matrix. However a slight decrease in mechanical strength and modulus are observed for 15 phr loading and this arises from the agglomeration of filler particles. These results are in good agreement with the SEM analysis. It can be seen that the elongation at break drops with increase in loading of nanoparticles and the reduction in elongation at break is considered as the criteria for higher reinforcement by nanoparticles [26]. Tear strength is an important property that reflects the resistance of composite towards crack growth. Table 2 showed an increase in tear strength up to 10 phr of  $\text{MnWO}_4$  and then showed a decrease with further loading of nanoparticles. This means that at 10 phr loading provides a large interfacial area of contact between nanoparticles and SBR matrix resulting in better interfacial adhesion. The abrasion resistance of SBR with different contents of nanoparticles are also reported in Table 2. The abrasion resistance increases with increase in loading of nanoparticles. The crystalline nanoparticles arrest the cracks or voids in the tip and thus increase the abrasion resistance. Better abrasion resistance

is observed for 10 phr filler loading and this improvement is probably due to the greater interfacial surface area and better filler-rubber interfacial adhesion. Rebound resilience of unfilled SBR is high as compared to filled composite and the resilience decreases continuously with the addition of nanoparticles. It is well known that the addition of inorganic fillers reduces the resilience. Hardness of composite material is a complex property and it depends on the concentration of filler particles in polymer. The variation in the hardness of composite given in Table 2, indicates that the hardness of materials increases progressively with the increase in loading of nanoparticles. Hardness of unfilled rubber is least in the series as expected. Generally a non-reinforcing filler shows lower compression set values as compared to a reinforcing particulate filler [27]. The compression set values of SBR/ $\text{MnWO}_4$  composite (Table 2) increases with increase in loading of filler particles. This can be attributed to the higher crosslink density of the composite. Heat build-up of an elastomer generated from the internal friction in the compounds. It can be seen from Table 2 that the heat build-up increases with the loading of nanoparticles, and this is because of the increased friction between the filler and elastomer.

### 3.8 Effect of Nanoparticles on Sorption and Diffusion with Petroleum Fuels

The sorption curves expressed as the mole percentage uptake ( $Q_t$ ) of petroleum fuels by 100 g of polymer against square root of time. Figure 6 shows the sorption curve of petrol through SBR/ $\text{MnWO}_4$  nanocomposite at room temperature. It is clearly seen that the solvent uptake of SBR is higher than that of SBR/ $\text{MnWO}_4$  nanocomposite. In the case of nanocomposite, the rate of solvent uptake is increases with the increase in loading of nanoparticles. The composite containing with 10 phr of filler loading shows the minimum solvent uptake. All the sorption experiments were conducted in petrol, diesel and kerosene. The solvent uptake of all the

**Table 2** Mechanical properties of SBR and SBR with various contents of  $\text{MnWO}_4$  nanoparticles

Properties	Loading of $\text{MnWO}_4$ nanoparticles (phr)					
	0	3	5	7	10	15
Tensile strength (MPa)	2.13	2.87	3.65	4.54	5.69	5.33
Elongation @ break (%)	425	412	399	383	370	351
Modulus (300%)	1.94	2.32	3.18	4.09	5.23	4.85
Tear strength (kN/m)	18	22	27	30	34	32
Hardness (Shore A)	33	35	36	37	39	42
Heat build-up ( $^{\circ}\text{C}$ )	10	11	12.3	13.5	14.9	16.4
Compression set (%)	19.8	18.9	18.01	17.6	17.0	16.2
Abrasion loss ( $\text{mm}^3$ )	66.8	66.4	66.2	66.0	65.7	65.9
Resilience (%)	46.24	45.89	44.96	44.05	43.59	43.01

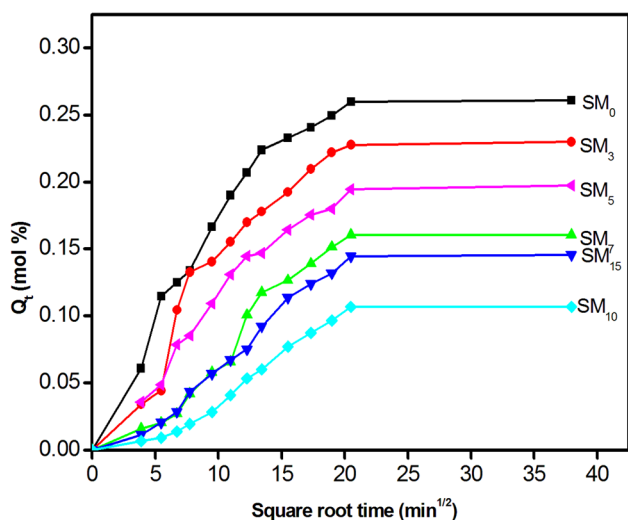


**Fig. 6** Sorption curves of SBR/MnWO<sub>4</sub> nanocomposite through petrol at room temperature

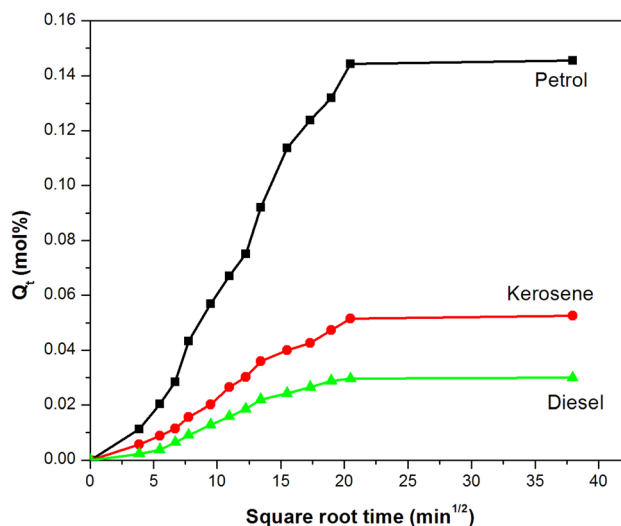


**Fig. 7** Solvent uptake of SBR with 10 phr of MnWO<sub>4</sub> in different industrial solvents

solvent followed the same diffusion trend. The minimum solvent uptake nanocomposite is mainly due to the formation of rigid regions in the matrix; which prevent the flexibility of the polymer [28]. Also the strong polymer-filler interaction leads to an orientation of nanoparticles within the polymer matrix (which is well clear from SEM analysis) and that reduces the solvent sensitivity of composites. The penetration of solvent molecule through polymer composite also depends on the free volume in the polymer matrix. When the loading of nanoparticles reached 15 phr, the solvent uptake slightly increases as compared to 10 phr loaded composite. The increase in solvent uptake is due to the poor dispersion of nanoparticles within SBR and that results in the agglomeration of nanoparticles in the matrix. This result also is in good agreement with AC conductivity and SEM analysis.

The effect of various solvents uptakes is investigated for composite with 10 phr loading of nanoparticles filled sample and this is given in Fig. 7. There is a systematic trend in the sorption behaviour of petroleum fuels with varying molecular weight of solvent. The decreases in  $Q_t$  with increase in molecular weight of solvent and is due to the high activation energy needed for the penetration of solvent molecule into elastomer matrix. The decrease in solvent uptake with increase in molar volume of penetrant has been reported by many researchers [29]. The diffusion rate strongly depends on the easy exchange of solvent molecules with polymer chains. The easy of exchange reduces as the penetrant size increases. Among the various petroleum fuels, the maximum and minimum  $Q_t$  values are shown by petrol and diesel respectively.

### 3.9 Effect of Temperature on Transport Properties

Here we select the composite with 10 phr loading of nanoparticles for studying the effect of temperature on solvent uptake and this is because of the better solvent resistance of composite at room temperature. Petrol is used as a solvent to study the effect of sorption and diffusion behaviour of SBR/10 phr MnWO<sub>4</sub> composite at different temperature such as 27, 40 and 50 °C. Figure 8 indicates the rate of diffusion and the equilibrium solvent uptake increases with the temperature. Moreover the slope of the initial linear position of the swelling curve increases with temperature. This is a clear indication that the transport process is

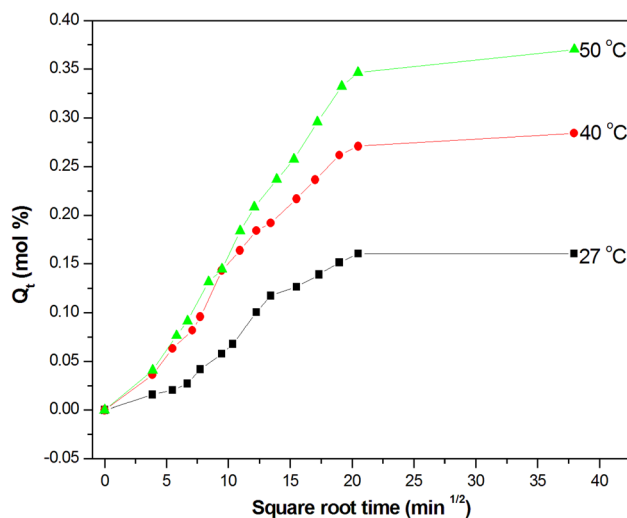


**Fig. 8** The mole uptake of SBR and SBR with 10 phr of MnWO<sub>4</sub> in petrol at different temperature



temperature dependent and activated. This is because of the increase in segmental motion of the polymer chain and it increases with temperature, which leads to the increase in free volume in the SBR matrix [30]. The temperature also enhances the collision of solvent molecules and thereby increases the kinetic energy of the system. All the composite shows the same behaviour with petrol as solvent.

The sorption (S), diffusion (D) and permeation coefficient (P) of composites in different solvents at room temperature is given in Table 3. The diffusion coefficient is a measure of better dispersion of nanoparticles in polymer matrix. This is a kinetic parameter, which explores about polymer segmental mobility and thus the rate of diffusion can be obtained using the following equation.

$$D = \pi \left( \frac{h\theta}{4Q_{\infty}} \right)$$

where  $h$  is the thickness of the sample,  $\theta$  the slope of the linear portion of the sorption curve of the plot of %  $Qt$  versus  $\sqrt{t}$ , and  $Q_{\infty}$  is the equilibrium absorption. On increasing the  $MnWO_4$  loading the free volume inside the composite decreases, hence the diffusion coefficient decreases with filler loading. This is due to better dispersion of nanoparticles in the composites, which is well understood from the SEM images (Fig. 2). The increased interfacial interaction between polymer and nanoparticles is revealed from the diffusion coefficient values. Its value decreases with increase in penetrant size is also explained on the basis of activation energy. High activation energy is needed for the penetration of high density solvents. These results are

in consistent with the previous work [31]. On comparing the diffusivity of SBR with 10 phr of  $MnWO_4$  in different solvents, the diffusivity is decreasing with increasing penetrant size, which well explained from Fig. 7. The sorption coefficient (S) also shows the similar trend as that of diffusion coefficient (D) of the composite materials. Sorption coefficient is a measure of the ratio of mass of the solvent at equilibrium swelling and the initial mass of the polymer sample. The permeation coefficient (P) depends on both diffusion coefficient and sorption coefficient, which is the amount of solvent permeated in to the composite in unit area per second. And is calculated as  $P=D \times S$ . From the table it is clear that D, S and P values decreases with the loading of nanoparticles, and the minimum value is exhibited by SBR/ $MnWO_4$  composite with 10 phr of nanoparticles. The slight increase in value for 15 phr sample is again explained according to the agglomeration found in SEM analysis.

The mechanism of transport can be calculated from the swelling data by using the equation

$$\log \frac{Qt}{Q_{\infty}} = \log k + n \log t$$

where  $Qt$  and  $Q_{\infty}$  are the mol% sorption at time  $t$ , and at equilibrium respectively,  $k$  indicates the interaction between the penetrant and the polymer and  $n$  represents the mode of transport. Here the value of  $n$  indicates that upon increasing the loading of nanoparticles, the composite first changes from a less Fickian to more Fickian mode of transport [32]. From Table 4 it is seen that the majority

**Table 3** D, S and P values of SBR  $MnWO_4$  nanocomposites in industrial solvents

Samples	Diffusion coefficient $D \times 10^5$ (cm <sup>2</sup> /s)			Sorption coefficient S (mol %)			Permeation coefficient $P \times 10^5$ (cm <sup>2</sup> /s)		
	Petrol	Kerosene	Diesel	Petrol	Kerosene	Diesel	Petrol	Kerosene	Diesel
SM <sub>0</sub>	1.53	1.39	1.28	1.20	1.19	1.17	1.83	1.65	1.49
SM <sub>3</sub>	1.41	1.28	1.22	1.18	1.16	1.15	1.66	1.48	1.41
SM <sub>5</sub>	1.36	1.21	1.18	1.13	1.11	1.09	1.53	1.34	1.28
SM <sub>7</sub>	1.22	1.17	1.14	1.12	1.08	1.08	1.36	1.26	1.23
SM <sub>10</sub>	1.03	0.99	0.91	1.05	1.02	0.92	1.08	1.01	0.83
SM <sub>15</sub>	1.09	1.07	1.03	1.09	1.06	1.02	1.18	1.13	1.05

**Table 4** The values of  $n$  and  $k$  of SBR/ $MnWO_4$  with different filler loading in industrial solvents at room temperature

Samples	Petrol		Kerosene		Diesel	
	$n$	$K \times 10^2$ (min <sup>-1</sup> )	$n$	$K \times 10^2$ (min <sup>-1</sup> )	$n$	$K \times 10^2$ (min <sup>-1</sup> )
MS <sub>0</sub>	0.32	0.32	0.56	0.21	0.62	0.19
SM <sub>3</sub>	0.44	0.31	0.73	0.14	0.76	0.12
SM <sub>5</sub>	0.63	0.18	0.61	0.19	0.69	0.16
SM <sub>7</sub>	0.61	0.17	0.60	0.17	0.66	0.19
SM <sub>10</sub>	0.63	0.18	0.56	0.21	0.63	0.18
SM <sub>15</sub>	0.75	0.13	0.49	0.27	0.62	0.19

of the composites approaches an anomalous mode of transport and all the values are found to be greater than 0.6. The variation from Fickian to anomalous mode indicates the increased swelling stress associated with the reinforcement. On increasing the amount of filler, the restriction towards the rearrangement of polymer chain increases. Polymer chain relaxation slows down and this leads to an anomalous mode of transport. This proves the improved interfacial interaction between polymer matrix and nanoparticles. The value of *k* reveals the structural properties of the polymer, and this gives an idea about the solvent-polymer interaction. Upon the addition of filler, the value of *k* decreases and that proves the strong interaction between polymer and filler, which will reduce polymer–solvent interaction [33].

Activation energy of sorption can be calculated using the Arrhenius equation

$$X = X_0 \exp\left(\frac{-E_X}{RT}\right)$$

where *X* is D or P, and *X*<sub>0</sub> is D<sub>0</sub> or P<sub>0</sub>, *E*<sub>*X*</sub> is the activation energy. From the plots of log D or logP against 1/*T* and from the slopes of curves the activation energy for diffusion (*E*<sub>D</sub>) and activation energy for permeation (*E*<sub>P</sub>) are calculated and presented in Table 5. Values of *E*<sub>P</sub> and *E*<sub>D</sub> for different industrial solvents are found to be increasing with the amount of nanoparticles and the size of the penetrant molecule. Similar results are observed for other researchers [34, 35]. In order to create a larger space for larger molecules inside the polymer composite requires higher activation. The better distribution of nanoparticles induces a higher resistance to solvent interaction. Hence, here the

better activation energy is obtained for SBR with 10 phr of MnWO<sub>4</sub>. The least value is noted for pure SBR. The enthalpy of sorption ( $\Delta H$ ) is calculated from the equation.

$$\Delta H = E_p - E_D$$

The  $\Delta H$  values also increase with increase in nanoparticle concentration. The endothermic nature of sorption is well established from the positive values of  $\Delta H$ .

Thermodynamic parameters such as  $\Delta H_s$  and  $\Delta S_s$  can be calculated from Van't Hoff's relation

$$\log K_s = \frac{\Delta S_s}{2.303R} - \frac{\Delta H_s}{2.303RT}$$

where *K*<sub>s</sub> is the equilibrium sorption constant, which is the ratio of number of moles of solvent sorbed at equilibrium to the mass of the polymer sample. On regression analysis of log *K*<sub>s</sub> against 1/*T* the values of  $\Delta H$  and  $\Delta S$  are obtained. Table 6 shows the thermodynamic properties of SBR and SBR/MnWO<sub>4</sub> composite with various nano-filler loadings for different industrial solvents. It is observed from the table that the all the samples in all solvent shows positive  $\Delta H$  values, which assures the endothermic mode of sorption. According to Henry's law, the sorption occurs with the creation of new holes or free space in the polymer matrix [36]. The entropy change ( $\Delta S$ ) values are positive, and it is seen that upon increasing the amount of MnWO<sub>4</sub> concentration,  $\Delta S$  values decreases. This is due to the increased interfacial interaction between polymer matrix and nanoparticles. The resulting reduction in entropy reduces the solvent transport [37]. The  $\Delta G$  values are increased from pure SBR to its composites, and the maximum value is noted for SBR with

**Table 5** *E*<sub>D</sub> and *E*<sub>P</sub> (kJ mol<sup>-1</sup>) values of SBR-MnWO<sub>4</sub> nanocomposites in different industrial solvents

Samples	Petrol			Kerosene			Diesel		
	<i>E</i> <sub>D</sub>	<i>E</i> <sub>P</sub>	$\Delta H$	<i>E</i> <sub>D</sub>	<i>E</i> <sub>P</sub>	$\Delta H$	<i>E</i> <sub>D</sub>	<i>E</i> <sub>P</sub>	$\Delta H$
MS <sub>0</sub>	3.55	4.19	0.64	3.93	4.69	0.76	4.6	5.42	0.82
SM <sub>3</sub>	4.39	5.37	0.98	4.49	5.39	0.9	4.56	6.11	1.55
SM <sub>5</sub>	5.87	7.01	1.14	6.11	7.42	1.31	7.01	8.87	1.92
SM <sub>7</sub>	5.89	7.24	1.16	6.27	7.65	1.41	7.13	9.05	2.08
SM <sub>10</sub>	6.20	7.46	1.26	6.44	8.28	1.84	7.56	9.58	2.22
SM <sub>15</sub>	6.09	7.28	1.18	6.32	7.78	1.46	7.24	9.12	2.18

**Table 6**  $\Delta H$ ,  $\Delta S$  and  $\Delta G$  (kJ mol<sup>-1</sup>) values of SBR-MnWO<sub>4</sub> nanocomposites in various industrial solvents

Samples	$\Delta H$			$\Delta S$			$-\Delta G$		
	Petrol	Kerosene	Diesel	Petrol	Kerosene	Diesel	Petrol	Kerosene	Diesel
S <sub>0</sub>	0.632	0.664	0.95	0.072	0.052	0.049	20.97	14.93	14.65
SM <sub>3</sub>	0.811	0.88	0.98	0.062	0.051	0.041	17.78	14.42	11.32
SM <sub>5</sub>	0.885	0.998	1.14	0.051	0.038	0.029	14.42	10.4	7.56
SM <sub>7</sub>	0.898	1.16	1.29	0.047	0.034	0.025	13.2	9.04	6.21
SM <sub>10</sub>	0.959	1.32	1.49	0.033	0.027	0.018	8.94	6.78	3.91
SM <sub>15</sub>	0.917	1.26	1.33	0.041	0.031	0.021	11.38	8.04	4.97

10 phr of  $\text{MnWO}_4$  nanoparticles. So the sorption is more spontaneous in pure SBR and on going from SBR to its composites, the spontaneity lowers and is least for 10 phr of composite. All these thermodynamic properties revealed the better distribution and strong interaction of SBR and  $\text{MnWO}_4$  nanoparticles.

#### 4 Conclusions

The present study investigated the effect of loading (3–15 phr) of  $\text{MnWO}_4$  nanoparticles on the morphology, crystalline nature, thermal stability, processing characteristics, interaction with petroleum fuels, mechanical and electrical properties of SBR composite. The XRD pattern of nanocomposite showed the decrease in amorphous nature of SBR by the interaction with  $\text{MnWO}_4$  nanoparticles. The uniform dispersion of nanoparticles in SBR decreased with an increase in the nanoparticles loading. The interactions of nanoparticles with SBR can effectively enhance the thermal stability of SBR. AC electrical conductivity and dielectric property of nanocomposites were higher than that of SBR and the maximum electrical property was obtained for 10 phr loading of nanoparticles. Above this loading, the electrical properties were found to decrease. Processing characteristics such as optimum cure time and scorch time decrease with the loading of  $\text{MnWO}_4$ , whereas the rheometric torque increased with loading of nanoparticles up to 10 phr. Addition of nanoparticles to SBR increased the tensile strength, modulus, tear, abrasion resistance, hardness and heat build-up, while elongation at break, resilience and compression set decreased. The liquid transport characteristics of nanocomposite were analysed using petrol, diesel and kerosene and the results were compared with that of unfilled SBR vulcanizates. Nanocomposites showed reduced penetration of solvent due to better interaction between nanoparticles and SBR. The solvent uptake was lower for 10 phr loading and the equilibrium solvent uptake increased at higher filler loading. This could be attributed to the poor interaction between the matrix and nano-filler that resulted in aggregation of nanoparticles. The sorption coefficient and activation parameter showed a dependence on the size of penetrant molecules. The transport phenomenon was found to follow anomalous type mechanism in all the cases. So the SBR/  $\text{MnWO}_4$  composite showed the significant improvement in the mechanical electrical and solvent sorption properties for 10 phr loading of nanoparticles.

**Acknowledgements** The authors wish to thank Prof. P. P. Pradyumnan, Department of Physics, University of Calicut, and Prof. P. Pradeep, Department of Physics, NIT Calicut, for providing necessary facilities in the department.

#### References

1. S. Al-Hussaini, W. Eldars, *J. Inorg. Organomet. Polym.* **26**, 691 (2016)
2. M.T. Ramesan, *J. Appl. Polym. Sci.* **131**, 3681 (2014)
3. H. Shahrajabian, S.Y.A. Brooghani, S.J. Ahmadi, *J. Inorg. Organomet. Polym.* **23**, 1282 (2013)
4. K.W. Park, G.H. Kim, *J. Appl. Polym. Sci.* **112**, 1845 (2009)
5. H. Zou, Q. Ma, Y. Tian, S. Wu, J. Shen, *Polym. Compos.* **27**, 529 (2006)
6. K. Suhailath, M.T. Ramesan, B. Naufal, P. Periyat, V.C. Jasna, P. Jayakrishnan, *Polym. Bull.* **74**, 671 (2017)
7. M.T. Ramesan, P. Jayakrishnan, *J. Inorg. Organomet. Polym.* **27**, 143 (2017)
8. A. Nihmath, M.T. Ramesan, *J. Inorg. Organomet. Polym.* **27**, 481 (2017)
9. M. Krook, A.C. Albertsson, U.W. Gedde, M.S. Hedenqvist, *Polym. Eng. Sci.* **42**, 1238 (2002)
10. M. Maiti, A.K. Bhowmick, *J. Appl. Polym. Sci.* **105**, 435 (2007)
11. J. H. Chang, Y.U. An, *J. Polym. Sci. B* **40**, 670 (2002)
12. M.T. Ramesan, *Int. J. Plast. Technol.* **19**, 368 (2015)
13. C.K. Radhakrishnan, B. Ganesh, A. Sujith, G. Unnikrishnan, S. Thomas, *Polym. Polym. Comp.* **13**, 335 (2005)
14. J.L. Leblanc, *Prog. Polym. Sci.* **27**, 627 (2002)
15. F. El-Tantawy, *Polym. Degrad. Stab.* **73**, 289 (2001)
16. M.T. Ramesan, K. Surya, *Polym. Renew. Resour.* **7**, 81 (2016)
17. S.S. Choi, *J. Appl. Polym. Sci.* **93**, 1001 (2004)
18. M.T. Ramesan, R. Alex, *Kautsch. Gummi Kunstst.* **53**, 596 (2000)
19. R.J. Kalbasi, N. Mosaddegh, *J. Inorg. Organomet. Polym.* **22**, 404 (2012)
20. M.T. Ramesan, V.P.A. Raheem, P. Jayakrishnan, P.P. Pradyumnan, *AIP Conf. Proc.* **1620**, 3 (2014)
21. S. Muthamizh, R. Suresh, K. Giribabu, R. Manigandan, S.P. Kumar, S. Munusamy, V. Narayanan, *J. Alloys Compd.* **619**, 601 (2015)
22. M.T. Ramesan, V. Nidhisha, P. Jayakrishnan, *Polym. Int.* **66**, 548 (2017)
23. P. Jayakrishnan, M.T. Ramesan, *J. Inorg. Organomet. Polym.* **27**, 323 (2017)
24. R.M. Mors, M.N. Ismaiel, A.A. Yehia, *Int. J. Mater. Meth. Tech.* **1**, 22 (2013)
25. M.T. Ramesan *Int. J. Polym. Mater.* **60**, 1130 (2011)
26. M.T. Ramesan, *J. Polym. Res.* **11**, 333 (2004)
27. M.T. Ramesan, *J. Elastom. Plast.* **46**, 303 (2014)
28. C. Sareena, M.T. Ramesan, E. Purushothaman, *Fibers Polym.* **14**, 1674 (2013)
29. M.T. Ramesan, *Polym. Polym. Compos.* **23**, 85 (2015)
30. C. Sareena, M.T. Ramesan, E. Purushothaman, *Polym. Compos.* **33**, 1678 (2012)
31. M.T. Ramesan, *Pet. Sci. Technol.* **32**, 1775 (2014)
32. M. Balachandran, S.S. Bhagawan, *J. Polym. Res.* **19**, 1 (2012)
33. A. Sujith, G. Unnikrishnan, *J. Mater. Sci.* **40**, 4625 (2005)
34. P. Mathew, S. Packirisamy, M.G. Kumaran, S. Thomas, *Polymer* **25**, 4935 (2002)
35. K.K. Hwang, S.H. Ryu, S.K. Hong, *J. Appl. Polym. Sci.* **86**, 2701 (2002)
36. V.S. Vinod, S. Varghese, B. Kuriakose, *J. Mater. Sci.* **35**, 5699 (2000)
37. J. Abraham, H.J. Maria, S.C. George, N. Kalarikkal, S. Thomas, *Phys. Chem. Chem. Phys.* **17**, 11217 (2015)